C-Terminal Truncation and Histidine-Tagging of Cytochrome *c* Oxidase Subunit II Reveals the Native Processing Site, Shows Involvement of the C-Terminus in Cytochrome *c* Binding, and Improves the Assay for Proton Pumping†

Carrie Hiser,‡ Denise A. Mills,‡ Michael Schall,‡,§ and Shelagh Ferguson-Miller*,‡

Department of Biochemistry and MSU-NIH Mass Spectrometry Facility, Michigan State University, East Lansing, Michigan 48824-1319

Received August 11, 2000; Revised Manuscript Received November 9, 2000

ABSTRACT: To enable metal affinity purification of cytochrome *c* oxidase reconstituted into phospholipid vesicles, a histidine-tag was engineered onto the C-terminal end of the *Rhodobacter sphaeroides* cytochrome *c* oxidase subunit II. Characterization of the natively processed wildtype oxidase and artificially processed forms (truncated with and without a his-tag) reveals *K*m values for cytochrome *c* that are 6−14-fold higher for the truncated and his-tagged forms than for the wildtype. This lowered ability to bind cytochrome *c* indicates a previously undetected role for the C-terminus in cytochrome *c* binding and is mimicked by reduced affinity for an FPLC anion exchange column. The elution profiles and kinetics indicate that the removal of 16 amino acids from the C-terminus, predicted from the known processing site of the *Paracoccus denitrificans* oxidase, does not produce the same enzyme as the native processing reaction. MALDI-TOF MS data show the true C-terminus of subunit II is at serine 290, three amino acids longer than expected. When the his-tagged form is reconstituted into lipid vesicles and further purified by metal affinity chromatography, significant improvement is observed in proton pumping analysis by the stopped-flow method. The improved kinetic results are attributed to a homogeneous, correctly oriented vesicle population with higher activity and less buffering from extraneous lipids.

Cytochrome *c* oxidase, the final electron acceptor in the respiratory chains of eukaryotes and many prokaryotes, catalyzes the reduction of oxygen to water and uses the energy available to pump protons across the membrane in which it is situated. The mechanism of the pumping process is not yet understood, but important insights have been gained by studying mutant forms of *Rhodobacter sphaeroides* oxidase reconstituted into phospholipid vesicles (*1*−*7*). In these studies, external pH changes are measured spectrophotometrically with the pH-sensitive dye phenol red (*8*, *9*). When measuring the very small pH changes involved, signal-to-noise is always a problem and is exacerbated by the buffering and light scattering effects of excess phospholipids. A high ratio of lipid to protein is required for good reconstitution, but it would be useful to be able to remove the excess lipids in empty vesicles and concentrate the oxidase-containing vesicles (COVs).[1] Several methods have been tried [sucrose gradient centrifugation (*10*) cytochrome *c* affinity chromatography (*11*)], but none have been completely satisfactory or reproducibly successful.

Addition of six histidines (a "his-tag") to the C-terminus of subunit I of the *R. sphaeroides* aa_3 oxidase (*12*) has greatly simplified purification of wildtype and mutant forms of CcO by Ni^{2+}-NTA affinity chromatography (*4*, *13*). However, when CcO is reconstituted and correctly oriented in vesicles, this his-tag is on the inside of the vesicles and is not available to allow further purification of the oxidase-containing vesicles by a metal affinity column. A form of the *R. sphaeroides* CcO was therefore constructed with the his-tag on the C-terminus of subunit II, which is on the exterior when the oxidase is reconstituted. The properties of this enzyme (htIICcO), as well as a control construct with a C-terminal deletion (htICcO-16) were studied and metal affinity chromatography was used to concentrate and purify COVs with oxidase correctly incorporated.

MATERIALS AND METHODS

Removal of the C-Terminus of Subunit II and Addition of the 6-Histidine Tag. The *R. sphaeroides* operon carrying the *cox*II-ORF1-ORF3-*cox*III genes was subcloned as a *Pst*I fragment from plasmid pYJ100 (*13*) into pUC119. The Muta-Gene Phagemid In Vitro Mutagenesis kit (Bio-Rad) was used

† Supported by NIH-RO1-GM26916 to S.F.M.

* To whom correspondence should be addressed. Telephone: 517-353-0199; fax: 517-353-9334; e-mail: fergus20@pilot.msu.edu.

‡ Department of Biochemistry.

§ MSU-NIH Mass Spectrometry Facility.

[1] Abbreviations: CcO, cytochrome *c* oxidase; COVs, cytochrome oxidase-containing phospholipid vesicles; CCCP, carbonyl cyanide *m*-chlorophenylhydrazine; FPLC, fast pressure liquid chromatography; HEPES, 4-(2-hydroxyethyl)-1-piperazineethanesulfonic acid; htICcO, wildtype *R. sphaeroides* oxidase enzyme with a 6-histidine tag on the C-terminus of subunit I; htICcO-16, *R. sphaeroides* oxidase enzyme with a his-tag on subunit I and 16 amino acids removed from the C-terminus of subunit II; htIICcO, *R. sphaeroides* oxidase enzyme with 22 amino acids removed from and a 6-histidine tag added to the C-terminus of subunit II; htII COVs, COVs containing the subunit II-his-tagged CcO; LM, lauryl maltoside; MALDI-TOF MS, matrix-assisted laser desorption time-of-flight mass spectrometry; ORF, open reading frame; Ni^{2+}-NTA, nickel-nitrilotriacetic acid; PCR, polymerase chain reaction; RCR, respiratory control ratio; SDS−PAGE, sodium dodecyl sulfate−polyacrylamide gel electrophoresis.

10.1021/bi0018988 CCC: $20.00
Published on Web 01/16/2001

to insert a unique *Sph*I site upstream of the *cox*II coding region and to remove the *Bam*HI site in ORF1, thereby making the *Bam*HI site just downstream of the *cox*II coding region unique. The *cox*II gene could then be removed from the operon for mutagenesis and subsequently replaced. A PCR-based mutagenesis method (*14*) utilizing Pfu polymerase was used to delete 16 amino acids from the C-terminus of subunit II or to delete 22 amino acids from the C-terminus and add six histidines. All mutagenesis primers were synthesized by the Macromolecular Structure Facility in the MSU Biochemistry Department, and all mutated fragments were subsequently sequenced by the MSU-DNA Sequencing Facility. After mutagenesis, the *cox*II gene was returned to its operon, which was then cloned into the *Pst*I site of the broad host range plasmid pRK415−1 (*15*). A his-tagged *cox*I gene from plasmid pJS3-SH (*4*) was added to the plasmid with the C-terminal-deleted *cox*II operon, resulting in the expression plasmid pCH25. A non-his-tagged *cox*I gene from plasmid pJS3 (*16*) was added to the plasmid with the subunit II-his-tagged operon, resulting in the expression plasmid pCH37.

The expression plasmids were transferred to *R. sphaeroides* strain YZ200 (*13*), which lacks the chromosomal copy of the coxII−III operon, by biparental conjugation as described (*17*) except omitting the incubation with bacteriophage T4. The resulting strains of *R. sphaeroides* were called: 25-1, expressing an oxidase with 16 amino acids deleted from the C-terminal of subunit II and retaining the his-tag on subunit I (htICcO-16), and 37-2, expressing an oxidase with 22 amino acids deleted and a his-tag added to the C-terminus of subunit II (htIICcO). A "wildtype" overexpressing strain YZ300 (*13*), which produces an oxidase with native subunit II and a his-tagged subunit I (htICcO), was used for comparison in some experiments.

Growth of Rhodobacter sphaeroides and Purification of Oxidase. Rhodobacter sphaeroides strains were grown in 2.8-L Fernbach flasks containing 600 mL of Sistrom's media (*18*) with 50 μg mL^{-1} streptomycin, 50 μg mL^{-1} spectinomycin, and 1 μg mL^{-1} tetracycline. The cultures were grown at 30 °C, shaken at 250 rpm, and harvested at an optical density at 600 nm of 1.5−1.8 and pH of 8.5−8.9. Cell membranes were prepared as described (*13*) except that, for strain 37-2, the concentration of KCl in the buffers was increased from 40 to 200 mM.

For metal affinity column purification, 10 mM imidazole was added to the solublized membranes in 10 mM Tris, pH 8.0, 2% LM, 40 mM KCl, which were then mixed with Ni^{2+}-NTA agarose resin (Qiagen) at a ratio of 1 mL of packed resin/mg of CcO. After the sample was stirred at 4 °C for 1 h, the mixture was poured into a column and washed with approximately 10 bed volumes of 10 mM Tris, pH 8.0, 0.1% LM, 40 mM KCl (= low-salt buffer) with 10 mM imidazole for strains 25-1 and YZ300 or with additional salt (to 200 mM KCl) (= high-salt buffer) for strain 37-2, followed by 5 to 10 bed volumes of buffer without imidazole. All CcO were eluted slowly with the low-salt buffer containing 80 mM histidine, then concentrated and washed three times with the low-salt buffer in an Ultrafree-15 centrifugal filter unit (Millipore) to remove histidine and nickel. The concentrated CcO was stored at −80 °C.

For further purification, 0.5−5 mg of CcO were diluted up to 0.2−2 mL with buffer A (10 mM KH_2PO_4, 1 mM EDTA, 0.2% LM, pH 7.2), made 3% in LM, and loaded onto tandem DEAE-5PW columns (Toso-HaaS) attached to an FPLC system (Amersham-Pharmacia Biotech AKTA-519). The columns were washed with buffer A, and the CcO was eluted at a flow rate of 0.5 mL min^{-1} with a gradient of buffer B (buffer A with 1 M KCl). For "standard" programmed conditions, the gradient was rapidly increased from 0 to 15% buffer B over 0.5 column volumes, and then the oxidase was eluted as the gradient was slowly increased from 15 to 45% buffer B over 4 column volumes. For some experiments, the pH of the buffers was changed to 8.0 or 9.0, or the gradient was held constant when a certain concentration of buffer B was reached, as described in the text.

Analysis of the Isolated Oxidase. Visible spectra were recorded on a Perkin-Elmer Lambda 40P spectrophotometer after appropriate dilutions of CcO into 100 mM KH_2PO_4, 0.1% LM, pH 7.2. The extinction coefficient used was $\Delta\epsilon_{606-650} = 41$ cm^{-1} mM^{-1} for dithionite-reduced oxidase (*19*). Maximal rates of oxygen consumption by 0.001 to 0.05 nmol of CcO were measured polarographically in 50 mM KH_2PO_4, pH 6.5, with 30 μM horse heart cytochrome *c* as the substrate and turnover numbers were calculated as described (*19*). The steady-state kinetics of cytochrome *c* reaction with CcO was measured in 10 mM Tris acetate, pH 8, by using 0.1 to 40 μM *R. sphaeroides* cytochrome c_2 as the substrate as described (*7*). For these steady-state kinetics assays, 8−14 nM of CcO was used; the wildtype CcO (htICcO) was further purified by FPLC to remove the unprocessed form of subunit II before use in these assays.

SDS−PAGE urea gels were run as described (*20*) except that the samples (10 μg of CcO/lane) were not TCA-precipitated prior to loading on the gel and were electrophoresed at room temperature at 100 V. Gels were stained by microwaving for 2 min in Coomassie stain, then shaking for 5 min; gels were destained 3−4 times by microwaving for 2 min in 7.5% (v/v) acetic acid in water, and then shaking for 5 min. Polypeptide sizes were estimated from low-molecular weight range markers (Bio-Rad).

Mass Spectrometry. MALDI experiments were performed by using a Voyager-DE STR MALDI-TOF mass spectrometer (PerSeptive Biosystems, Framingham, MA) equipped with delayed ion extraction. The samples were irradiated with a N_2 laser at 337 nm, producing 3 ns wide pulses. The spectra were acquired in positive-ion linear mode at 25 kV initial acceleration voltage.

Samples were prepared with the dried-droplet method mixing 1 μL of sample, diluted in 60% formic acid, with 1 μL of sinapinic acid (Sigma) solution [10 mg mL^{-1}, acetonitrile-0.1% trifluoroacetic acid, 1:1 (v/v)] directly on the target. Myoglobin and myoglobin dimer were used as external standards. The known mass of the "artificially processed" htICcO-16 cytochrome *c* oxidase subunit II was used to assess the accuracy of the mass of the natively processed subunit II.

Reconstitution of Oxidase into Vesicles and Purification of COVs. To prepare for reconstitution, 40 mg mL^{-1} asolectin lipids (purified as in Sone et al., 1997) were suspended in 2% cholate (Anatrace), 75 mM HEPES-KOH, pH 7.4, and sonicated to clarity. Four micromolar oxidase was incubated with 75 mM HEPES-KOH, pH 7.4, and 4% cholate on ice

for 1 h. Equal volumes of lipids and oxidase were mixed to give a final concentration of 2 μM oxidase and 20 mg mL^{-1} lipid (*19*).

For htIICcO, the cholate was removed by passage through a 1.4 × 40 cm (70 mL volume) Sephadex G-25 column equilibrated with 200 mL (approximately 3 column volumes) of 75 mM HEPES-KOH, pH 7.4, 14 mM KCl. The eluted vesicle fractions were diluted 1:1 with 20 mM HEPES-KOH, pH 8.0, 27 mM KCl, and 38 mM sucrose, and the pH was adjusted to 8.0 with KOH before addition to Ni^{2+}-NTA agarose at a ratio of 1 mL of COVs to 2 mL of packed resin washed in the same buffer. After the sample was stirred for 1 h at 4 °C, the resin was poured into a column and washed with 10 mL of the pH 8.0 buffer. Vesicles containing correctly oriented oxidase bound to the column and were eluted with 20 mM HEPES-KOH, pH 7.4, 100 mM histidine, 38 mM sucrose. Histidine and buffer were removed by concentration of the COVs on a Centriplus 100 centrifugal spin filter (Amicon) and dialysis for 12 h against 1000 volumes of 50 μM HEPES-KOH, pH 7.4, 44 mM sucrose, 45 mM KCl, and 1 mM EDTA. The concentration of oxidase in the prepared vesicles was calculated from the dithionite reduced spectrum at 605 nm using an extinction coefficient of 33.35 mM^{-1} cm^{-1} after background baseline subtraction (*21*).

Proton Pumping Measurements. Proton pumping of the COVs was measured in a rapid scanning stopped-flow spectrophotometer (Olis RSM). Horse heart cytochrome *c* was prereduced with dithionite and desalted through a Sephadex G-75 column in 0.5 mM HEPES-KOH, pH 7.4, 45 mM KCl, 1 mM EDTA, and then concentrated to about 1 mM. The buffer for stopped-flow measurements was as for the last dialysis step (above) with the addition of 100 μM phenol red and 1 mM EDTA. Scans were collected (1000 s^{-1}), and from these, kinetic traces for cytochrome *c* oxidation at 550 nm or phenol red changes at 556.8 nm (isosbestic point of cytochrome *c*) were taken after averaging several data sets and creating the difference spectra (reduced minus oxidized). A small mixing artifact at 0−200 ms was subtracted from the phenol red changes. The small changes in phenol red absorbance and the spectral overlap with the absorbance of cytochrome *c* did not allow for Global deconvolution of the proton-transfer rates. Therefore, rates of proton uptake or release were measured by fitting the kinetic traces at the isosbestic point (556.8 nm) to one exponential with Microcal Origin. The cytochrome *c* oxidation rates were from Global fitting analysis by the Olis software to a single component exponential and were similar to those obtained from the kinetic traces at 550 nm, but the latter were perturbed by the influence of the phenol red absorbance and better fits were obtained with Global analysis to eliminate the dye contribution.

RESULTS

Construction of the C-Terminal-Deleted and Subunit II-His-Tagged Oxidases. To purify vesicles containing correctly oriented oxidase (COVs) by metal affinity chromatography, a form of the wildtype *R. sphaeroides* CcO with an external 6-histidine-tag (his-tag) was created. The his-tag was placed at the C-terminus of subunit II, normally located toward the periplasmic space in bacteria, and was expected to be external

ALIGNMENT OF C-TERMINI OF SUBUNITS II OF CcO

Bovine	207	MPIVLELVPL KYFEKWSASM L
Paracoccus	255	MPIVVKAVSQ EKYEAWLAGA KEEFAA**DASD YLPASPVKLA SAE**
R. sph. htICcO (gene sequence)	263	MPITVKVVSE EAYAAWLEQA RGG.TYELSS VLPATPAGVS VE
R. sph. htICcO (crystal structure)	263	MPITVKVVSE EAYAAWLEQA RGG.TYEL
R. sph. htICcO (mass spectrometry)	263	MPITVKVVSE EAYAAWLEQA RGG.TYELS
R. sph. htICcO-16	263	MPITVKVVSE EAYAAWLEQA RGG.TY
R. sph. htIICcO	263	MPITVKVVSE EAYAAWLEQH HHH.HH

FIGURE 1: Alignment of the C-terminal regions of cytochrome *c* oxidase subunits II. Sequences are compared from bovine heart (*23*); *Paracoccus denitrificans* (*22*, *24*); wildtype *Rhodobacter sphaeroides* (*R. sph*. htICcO) as predicted from the gene sequence (*17*), as seen in the unpublished crystal structure (Iwata, personal communication) and as discovered from MALDI-TOF-MS (this work); and the *R. sphaeroides* constructs with 16 amino acids removed from the C-terminus (htCcO-16; this work) and with 22 amino acids removed and 6 histidines added (htIICcO; this work). The processed portion of the *P. denitrificans* C-terminus is shown in bold type. The C-terminal helix of the bovine subunit II is underlined.

when the oxidase was reconstituted into COVs. There is evidence that the C-terminus of the *R. sphaeroides* subunit II is processed in a similar way as the closely related enzyme from *Paracoccus denitrificans* (Figure 1; *22*). In *R. sphaeroides* CcO, a doublet of subunit II polypeptides, differing by about 2000 Da in molecular mass, is routinely observed on SDS−PAGE gels (*13*, *19*; see also Figure 4, lane 1), suggesting incomplete processing. Complete deletion of the normally processed region was required before attaching the his-tag to prevent its removal. As a control for the his-tagged version, the 16 amino acids that were expected to be removed by normal processing were genetically removed from the C-terminus of subunit II. The resulting oxidase, htICcO-16, with an "artificially processed" subunit II and retaining a his-tagged subunit I, was fully active and had only a single subunit II polypeptide (see Figure 4, lanes 2 and 3).

In the first attempt to make the subunit II-his-tagged CcO, six histidines were added to the C-terminus of the htICcO-16 construct (Figure 1). This CcO was only produced in low amounts in *R. sphaeroides* membranes, did not bind well to the Ni^{2+}-NTA column, and had a spectrum with an alpha peak shifted to 600 nm (data not shown). These characteristics could be explained if the additional histidines beyond the natively processed C-terminus could fold down and interact with the face of subunit II so as to alter the structure to cause spectral changes.

In the second attempt, 6 more amino acids were removed from the C-terminus (minus 22 amino acids total). This is the point in bovine CcO at which the C-terminal helix of subunit II ends (Figure 1, underlined; *23*). Six histidines were then added at this point. The resulting oxidase, htIICcO, was successfully overproduced in *R. sphaeroides*. The reduced spectra of Ni^{2+}-NTA purified his-tagged oxidases are presented in Figure 2. The spectrum of htIICcO (solid line) is similar to that of htICcO-16 (dotted line), to wildtype htICcO (dashed line), and to a non-his-tagged wildtype CcO (*19*), showing normal peaks at 606 and 444 nm.

Figure 3 shows the location of the added subunit II his-tag (in red) modeled on the crystal structure of the *P. denitrificans* subunit II (*24*), which is expected to be similar

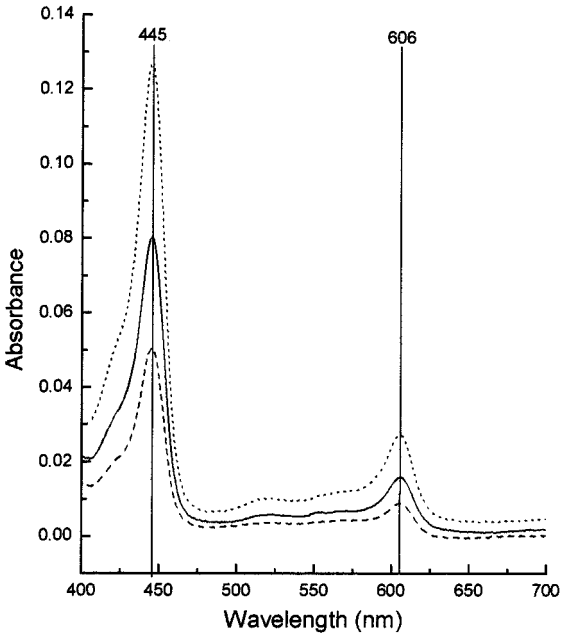

FIGURE 2: Spectra of dithionite-reduced cytochrome *c* oxidases from *Rhodobacter sphaeroides*. The oxidases from strains 25-1 (htICcO-16; dotted line), 37-2 (htIICcO; solid line), and YZ300 (wildtype htICcO; dashed line) were purified by using Ni^{2+}-NTA affinity chromatography. The Soret and alpha peaks at 445 and 606 nm are marked by lines.

to that of *R. sphaeroides* for which the crystal structure coordinates are not yet published. The his-tag is expected to be exposed on the external, soluble domain of subunit II, and therefore readily available for purification of the oxidase and COVs. However, higher concentrations of salt were necessary in the buffers used in metal affinity column purification to bind htIICcO. At the 40 mM KCl used in buffers for the isolation of htICcO, only 40−50% of htIICcO bound to the Ni^{2+}-NTA column, while at 200 mM KCl virtually 100% bound to the column. This suggests a lack of accessibility of the his-tag in the htIICcO at the lower salt concentration. We conclude that the his-tag may be interacting with the adjacent, negatively charged amino acids on the face of subunit II (shown in green in Figure 3). Increasing the salt concentration in the purification buffers provides better screening of charges, thereby keeping the his-tag more available for interaction with the metal on the resin.

Purification of the Subunit II-Modified Oxidases. Figure 4 shows an SDS−PAGE gel of the subunit II-modified CcO. As expected, these modified oxidases possessed only one subunit II polypeptide (lanes 2 and 3, htICcO-16; lanes 4 and 5, htIICcO) instead of the doublet seen in wildtype htICcO (lane 1). The slight size differences in subunits I and II between the different oxidases are explained by the locations of the his-tags.

Because of the use of higher salt in the Ni^{2+}-NTA column buffers, the htIICcO purified by the Ni^{2+}-NTA column alone (Figure 4, lane 4) was considerably less pure than the htICcO-16 purified by the Ni^{2+}-NTA column (lane 2). A single round of further purification by FPLC under our standard programmed conditions at pH 7.2 did not improve the purity of htIICcO very much (lane 5), although htICcO-16 was well-purified under these same conditions (lane 3). However, both of these oxidases still contained a 68-kDa polypeptide, which is a persistent contaminant in our preparations of *R. sphaeroides* CcO.

Consequently, a variety of conditions were tried to improve the purity of htIICcO. Holding the gradient at 19−20% buffer B in the FPLC purification (lane 6) improved the purity significantly but did not remove the 68-kDa polypeptide.

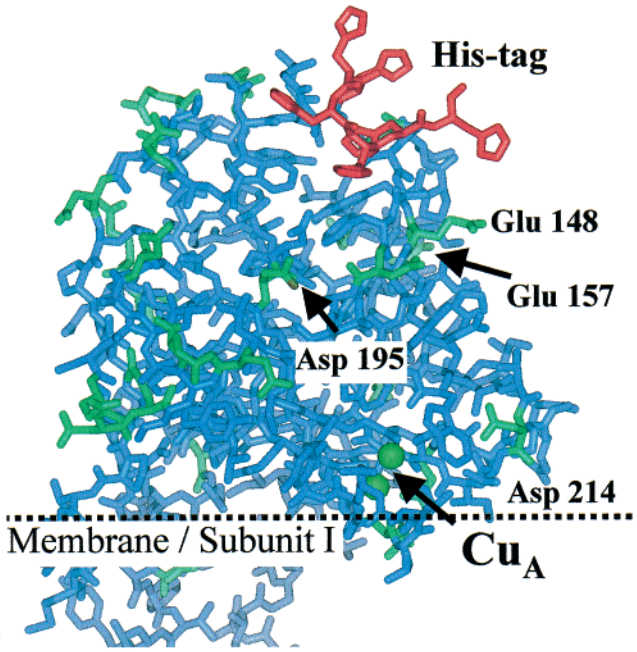

FIGURE 3: Model of the location of the added 6-histidine tag. The C-terminal his-tag (shown in red) added to the *Rhodobacter sphaeroides* cytochrome *c* oxidase subunit II sequence is modeled on the coordinates from the *Paracoccus denitrificans* crystal structure (*24*). Note that no particular secondary structure for the his-tag is implied by this diagram. Acidic residues on the face of subunit II that have been proposed to interact with cytochrome *c* (*7*) are labeled and shown in green.

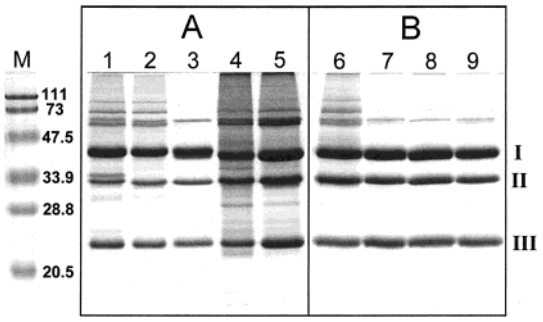

FIGURE 4: SDS−PAGE of various purified forms of *Rhodobacter sphaeroides* cytochrome *c* oxidases. Panel A compares different oxidases with and without FPLC purification under standard conditions. Lane 1: Ni^{2+}-NTA column purified wildtype htICcO, showing both processed and unprocessed forms of subunit II; lane 2: Ni^{2+}-NTA column purified htICcO-16; lane 3: htICcO-16 further purified by FPLC; lane 4: Ni^{2+}-NTA column purified htIICcO; lane 5: htIICcO further purified by FPLC. Panel B shows that varying the standard FPLC purification conditions improves purification of htIICcO. Lane 6: htIICcO purified by holding the gradient at 0.19−0.2 M KCl; lane 7: htIICcO purified by increasing the pH of both buffers to 8.0; lane 8: htIICcO purified by increasing the pH of both buffers to 8.0 and holding the gradient at 0.173 M KCl and again at 0.247 M KCl; lane 9: htIICcO purified by increasing the pH of both buffers to 9.0. M: low molecular weight range markers (Bio-Rad) with relative molecular weights given in kilodaltons. Subunits are numbered at the right.

Increasing the pH of all buffers to 8.0 (lane 7) or 9.0 (lane 9) gave much better separation than the standard conditions and removed most of the 68-kDa polypeptide. A combination of increasing the pH in all buffers to 8.0 and holding the gradient at 17.3% buffer B and again at 24.7% buffer B (lane 8) did not purify the htIICcO any better than the increase in pH alone. It should be noted that htIICcO was still highly active (turnover number of 1490 s^{-1}) even after purification at pH 9.0.

In the FPLC-DEAE purifications, the elution behaviors of both htICcO-16 and htIICcO were significantly different from the wildtype htICcO (Figure 5). The artificially processed htICcO-16 (curve 2, peak *) eluted much earlier in the gradient than either the processed (curve 1, peak *) or unprocessed (curve 1, arrow) forms of the wildtype htICcO. The subunit II-his-tagged htIICcO (curve 3, peak *) eluted even earlier than htICcO-16. Raising the pH from 7.2 to 8.0 (Figure 5, curve 4) or 9.0 (Figure 5, curve 5) resulted in much better retention of htIICcO, with the dramatically better removal of contaminants. This effect seemed likely to relate to a change in the charge on the subunit II-modified CcO, resulting from the artificial processing (removal of an extra negative charge) and the addition of the histidine tag (adding several partially positive charges).

Kinetic Characterization of the Subunit II-Modified Oxidases. The htICcO-16 and htIICcO proved to be similar to wildtype htICcO when assayed polarographically at low pH with excess substrate (pH 6.5, 30 μM horse heart cytochrome *c*), showing maximal turnover numbers of approximately 1500 and 1800 s^{-1}, respectively, as compared to approximately 1600−2000 s^{-1} for wildtype (*7*, *13*, *19*). However, both the need for higher salt in the Ni^{2+}-NTA column purification steps and the altered FPLC elution profiles suggested that the deletion of the C-terminus and the addition of the his-tag could be affecting the cytochrome

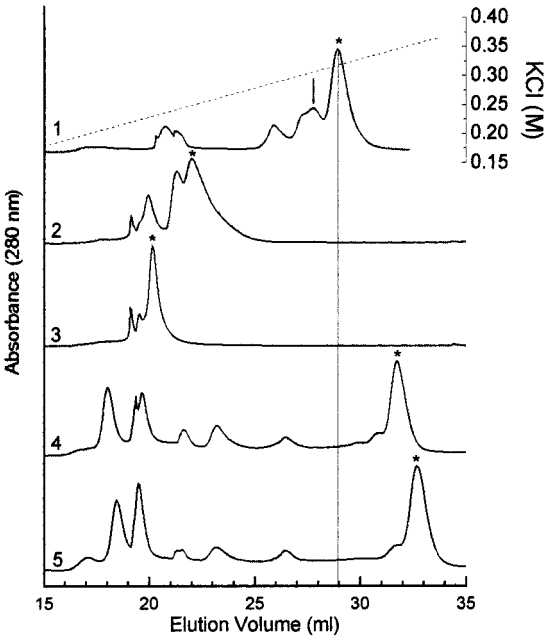

FIGURE 5: FPLC elution profiles of *Rhodobacter sphaeroides* cytochrome *c* oxidases purified under standard conditions and at different pHs. The elution volume in milliliters is plotted versus absorbance at 280 nm. Curve 1 is the wildtype htICcO (with natively processed and unprocessed forms of subunit II); curve 2 is htICcO-16 (with the artificially processed subunit II); curve 3 is htIICcO (with the subunit II his-tag). All were purified at pH 7.2. HtIICcO was also purified at pH 8.0 (curve 4) and pH 9.0 (curve 5). A total of 4.7 mg of oxidase was loaded for curve 2 and 0.5 mg oxidase was loaded for all other elution profiles. However, the curves were rescaled for easier viewing in this figure such that the tallest peaks were approximately the same height. The FPLC peaks containing the desired oxidases (used for the gel in Figure 4) are marked by asterisks on each curve. On curve 1, the arrow points to the form of the wildtype enzyme with the unprocessed subunit II; the asterisk indicates the form with a processed subunit II. The dotted line represents the gradient of KCl (right axis).

c binding face of subunit II, which might also be expected to alter the affinity of the interaction of the oxidase with cytochrome *c*, even though no activity changes were apparent under conditions of excess substrate.

To further investigate this possibility, the steady-state kinetics of the interactions of both htICcO-16 and htIICcO with *R. sphaeroides* cytochrome c_2 were measured polarographically at pH 8.0 (*7*). Figure 6 shows Eadie-Hofstee plots of htICcO-16 and htIICcO as compared to the natively processed form of wildtype htICcO. The nonlinear plots suggest the presence of two cytochrome c_2 binding sites (*25*), which can be analyzed according to the model presented by Zhen et al. (*7*) for high-affinity and low-affinity cytochrome *c* binding sites. The slopes of the dotted lines relate to the approximate *K*m values for the high-affinity interaction in each case: the steeper the slope, the higher the affinity and the lower the *K*m value. It is apparent that the wildtype htICcO has a higher affinity for cytochrome *c* than htICcO-16, which in turn has a higher affinity than htIICcO. The second, low affinity phase of the interaction, which is well defined in the case of wildtype htICcO, is barely indicated in the two mutant forms, suggesting that the second binding interaction is also much reduced in affinity or absent. Table 1 presents the Michaelis constants and the maximum rates (K_{m_1} and V_{max_1}) for the high-affinity phases of the reactions analyzed by the equation described in Zhen et al. (*7*). The

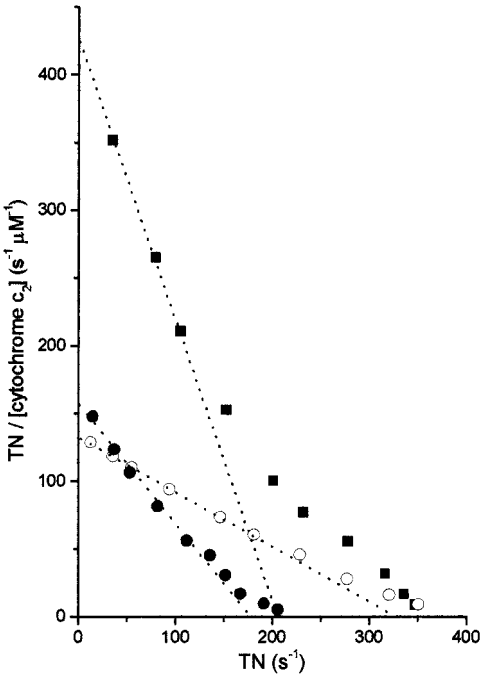

FIGURE 6: Steady-state kinetics profiles of cytochrome *c* oxidases. *Rhodobacter sphaeroides* cytochrome c_2 at 0.1 to 40 μM was used as the substrate. The turnover number (TN; *x*-axis) is plotted versus the TN divided by the concentration of cytochrome c_2 (*y*-axis). The steady-state kinetics of htICcO-16 (artificially processed subunit II; solid circles) and htIICcO (subunit II his-tagged; open circles) are compared to those of the wildtype htICcO (FPLC-purified form with only the natively processed subunit II; solid squares). Dotted lines represent the approximate slopes of the high-affinity phase of interaction.

Table 1: Comparison of the Kinetics of Differently Processed and His-Tag Labeled Cytochrome *c* Oxidases[a]

sample	FPLC purification	Km$_1$ (μM)	Vmax$_1$ (s^{-1})
htICcO[b]	yes	0.2 ± 0.1	92 ± 44
htICcO[c]	no	0.4 ± 0.1	144 ± 20
htICcO-16	no	1.2 ± 0.1	181 ± 10
htIICcO	no	2.5 ± 0.2	326 ± 18

[a] Steady-state kinetic data obtained by using 0.1 to 40 μM *Rhodobacter sphaeroides* cytochrome c_2 as the substrate were fitted to a model with two cytochrome *c* binding sites as described in ref *7*. The Vmax$_1$ is not the maximal turnover number of the enzyme, only the extrapolated turnover of the high affinity phase. The Km$_1$ refers to the high affinity phase. [b] This wildtype htICcO is the form containing the natively processed subunit II; it was isolated by using FPLC purification to remove the unprocessed form. [c] For comparison, we include data from ref *7* on wildtype htICcO containing a mixture of both processed and unprocessed forms of subunit II.

calculated values for the wildtype htICcO differ significantly from the estimates made from the slope of the line in Figure 6 due to the major contribution of the second phase to the first, which is corrected for by the kinetic analysis. The calculated Km$_1$ of the htIICcO is 14-fold higher than that of the wildtype htICcO, and the calculated Km$_1$ of htICcO-16 is 6-fold higher, indicating that both oxidases have significantly lower affinity for cytochrome c_2. Since the htICcO-16 was artificially processed to simulate the mature wildtype CcO (based on the known *P. denitrificans* processing site; *22*, *24*), it was expected to possess similar kinetics to the wildtype htICcO. However, the Km$_1$ and Vmax$_1$ are clearly different from the previously reported values (*7*) and

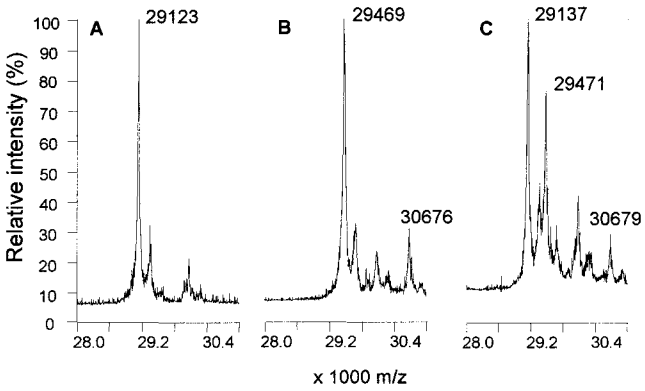

FIGURE 7: MALDI-TOF MS of the artificially processed htICcO-16 (panel A), FPLC-purified, natively processed wildtype htICcO (panel B), and a mixture of the two (panel C). The major peaks in the region of the spectrum shown are from subunit II, presumably because it is more effectively desorbed from the probe under the conditions used. The number shown for the major peak in panel A was determined by using myoglobin (16953) and myoglobin dimer (33904) as the standards. The numbers in panel B were calibrated to the known molecular mass of the artificially processed subunit II of htICcO-16. The numbers in panel C are internally calibrated to the known molecular ion of the artificially processed subunit II. See text for discussion of the identities of the peaks.

the values measured here (Figure 6 and Table 1). The results suggest that the artificially processed htICcO-16 is unlike the natively processed htICcO in a way that affects its interaction with both cytochrome *c* and DEAE-chromatography resin.

Mass Spectrometry of the C-Terminus of Subunit II. MALDI-TOF MS was performed on FPLC-purified wildtype htICcO and artificially processed htICcO-16 to determine the true C-terminus of the natively processed subunit II (Figure 7). Panel A shows the mass spectrometry profile of htICcO-16 oxidase, giving a major single charge peak with a molecular mass of 29 123, calibrated with standards of myoglobin (16 953) and myoglobin dimer (33 904). This peak can be identified, within 14 mass units, as the artificially truncated subunit II with a calculated mass of 29 136 (29 137 for the single charge molecular ion). Panel B shows the mass spectrometry profile of a wildtype htICcO sample, which was FPLC-purified and contained mostly natively processed subunit II as determined by SDS−PAGE (data not shown). The molecular ion masses were calibrated to the known mass of the artificially truncated subunit II. The major peak at 29 469 corresponds accurately with the calculated molecular ion mass (29 467) of a form that is natively processed three residues beyond the expected *P. denitrificans* cleavage site (Figure 1), after serine 290. It is significantly different from the calculated molecular ion masses of the artificially processed subunit II of htICcO-16 (29137) and from the C-terminal-unprocessed form (30 675). A small peak at 30 676, corresponding to the latter form, can be clearly identified in panel B but not in panel A, as expected.

In panel C, the two samples from panels A and B were mixed and run together as an internal calibration of the masses of the two native subunit II peptides against the artificially processed peptide. The molecular ion masses of the peaks were 29 137, artificially processed standard; 29 471, natively processed form; 30 679, unprocessed form. These values are within 4 mass units of the calculated values for these species, confirming that the native processing site

Table 2: Stopped-Flow Measurements of Electron Transfer Rates of Reconstituted HtII-CcO, Comparing Ni-Affinity Purified COVs with the Normal Preparation (See Figure 8)[a]

ht II COVs		rates of electron transfer (s^{-1})				
preparation	CcO (μM)	controlled	pumping (+ val)	uncontrolled (+ val + CCCP)	H^+/e^-[b]	RCR[c]
normal	0.26	70 ± 5	220 ± 8	390 ± 38	0.7	5.4
Ni-purified	0.23	100 ± 5	410 ± 35	690 ± 48	0.8	6.8
Ni-purified	0.09	90 ± 6	370 ± 60	1100 ± 39	0.8	12.0

[a] Normal reconstitution involves gel filtration to remove detergent; Ni-affinity purified COVs were treated the same but with additional Ni−NTA chromatography (see Materials and Methods). Rates (e^-/s/aa_3) of cytochrome *c* oxidation were obtained from global analysis of the data multiplied by [cyt c^{2+}]/[aa_3CcO], either with no ionophores (controlled), with valinomycin (proton pumping), or with valinomycin + CCCP (uncontrolled) with 5 μM cyt c^{2+}. Standard errors of the mean are shown for kinetic rates of the three individual traces averaged per measurement. [b] H^+/e^- = stoichiometry of protons pumped per electron transferred from the extent of absorbance change at 557 nm; acidification (+ valinomycin)/alkalinization (+ valino + CCCP) from Figure 8. [c] RCR = respiratory control ratio: the electron-transfer activity uncontrolled, divided by controlled.

in *Rhodobacter* is three amino acids beyond the one predicted from the *Paracoccus* sequence.

Characterization of the Reconstituted htIICcO Kinetics of Reaction with Cytochrome c. Reconstitution of the his-tag II oxidase into phospholipid vesicles and subsequent purification of the oxidase-containing vesicles (see Materials and Methods) resulted in COVs with good respiratory control (RCR = 6.8) similar to that with the normal dialysis method of vesicle preparation, and proton pumping was observed (Table 2). Removal of detergent is normally through a long dialysis protocol (*19*), but vesicles made with htIICcO did not bind adequately to Ni^{2+}-NTA unless detergent was removed rapidly by gel filtration. This may be because the COVs are smaller when prepared by this column method (*26*), with better curvature to expose the his-tag.

A comparison was made of htII COVs after reconstitution through Sephadex G-25 and a short dialysis step (Figure 8, panel A) and with the addition of a Ni^{2+}-NTA purification step (Figure 8, panel B). The H^+/e^- stoichiometries were similar, 0.7 and 0.8, respectively, when determined from the total absorbance changes (Table 2), but the rates of change of pH were markedly different, particularly in the alkalinization phase with uncoupler present.

The alkalinization (seen as an increase in absorbance of the phenol red) is observed when valinomycin and CCCP are present to allow leakage of K^+ and protons from the exterior bulk to the interior of the vesicles to compensate for the reduction of oxygen to water, resulting in a net one proton consumed for each electron used. This permits the change in absorbance during alkalinization to be used as a calibration for the phenol red changes seen during acidification with valinomycin alone. The observed rate of alkalinization in the metal affinity purified htII COVs (Figure 8, panel BI) was much faster than the nonmetal affinity purified. The slower alkalinization rate in the nonpurified htII COVs is probably caused by the excess presence of lipids (removed in the Ni^{2+}-NTA step) which act to buffer the protons, reduce the availability of cytochrome *c*, particularly when uncoupler makes the buffering of both the interior and the exterior of the vesicles available, and lessen the kinetic efficiency of valinomycin and uncoupler.

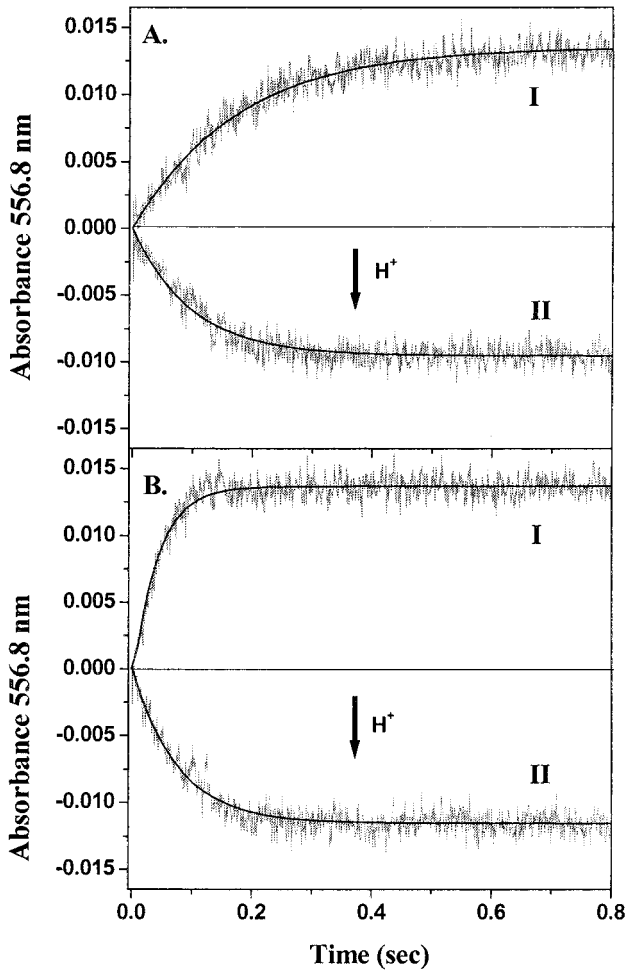

FIGURE 8: Proton pumping of Ni^{2+}-NTA purified htII COVs as compared to htII COVs not purified. Measurements were made in the Olis-rsm stopped-flow (see Materials and Methods) with 0.1 μM oxidase and 5.5 μM cytochrome c^{2+}. (A) Phenol red changes with htII COVs after removal of detergent by gel filtration (G-25) followed by concentration in a Centricon 100 and 2 × 1000 volume dialysis into the proton pumping buffer. (B) HtII COVs prepared as above but with additional Ni-NTA affinity column purification (see Materials and Methods). (I) Alkalinization (absorbance ↑ protons consumed) after uncoupling by the addition of 2 μM valinomycin + 5 μM CCCP. (II) Acidification (absorbance ↓ protons pumped outside) due to proton pumping in the presence of 2 μM valinomycin to alleviate build-up of the membrane potential.

From previous studies (*27*), the usual radius of vesicles prepared in this way is 150 Å, with 5−20 molecules of oxidase per vesicle (based on the subunit-III depleted bovine oxidase which is reasonably comparable in size to the *R. sphaeroides* oxidase). From calculations of amounts of lipid based on these parameters, and assuming only oxidase-containing vesicles are present in the purified samples, we expect that only 1−3 mg mL^{-1} of the original 20 mg mL^{-1} lipid remains in the Ni-NTA purified sample. This gives about a 10-fold decrease in buffering capacity.

A correlated difference in the purified htII COVs was their faster electron transfer rates observed by stopped flow (TN, apparent molecular activity) (Table 2). Some of the change may be due to the increased population of correctly oriented oxidase, even though about 80% are expected to be correctly oriented in the nonpurified COVs (*28*, *29*). More importantly, cytochrome *c* depletion by binding to the excess charged phospholipids (*30*), may reduce the initial cytochrome *c* rates

in the proton pumping measurements. This latter explanation is favored since similar turnover numbers are observed in the steady-state assay at high cytochrome *c* concentrations (1400 s^{-1}). Less kinetic efficiency of valinomycin and CCCP may also be a contributing factor in the stopped-flow analysis as compared to the steady-state. The uncontrolled rates of htII COVs appear to correlate with the level of lipid in the sample (see Table 2: highest lipid, TN = 390 s^{-1}; ~1/10th lipid, TN = 690 s^{-1}; ~1/25th lipid, TN = 1100 s^{-1}), as do the RCR values (Table 2). These observations confirm that excess lipid presents a substantial problem in obtaining dependable kinetic rates and control parameters in stopped-flow analysis.

The purified COVs also gave more reproducible rates and H^+/e^- stoichiometries than the unpurified (data not shown), but the expected improvement in signal-to-noise was not found, possibly because the small-sized vesicles are more light scattering in the stopped-flow.

DISCUSSION

Construction of the Subunit II-Modified Cytochrome c Oxidases. Both the *R. sphaeroides* aa_3 oxidase (*4*, *13*) and the *Escherichia coli* bo_3 oxidase (*12*, *31*) can be successfully purified by metal affinity chromatography by using a his-tag placed at the C-terminus of subunit I. When CcO is reconstituted into vesicles, however, this tag is internal and therefore inaccessible. With the aim of using Ni-affinity chromatography to purify vesicles that contain correctly oriented CcO, we created a form of the wildtype *R. sphaeroides* CcO with a 6-histidine tag at the C-terminal of subunit II that would be external when the oxidase is reconstituted.

To provide a control for the subunit II-his-tagged oxidase, we first constructed a strain to express htICcO-16, which has the C-terminus of subunit II "artificially processed" at the same point as the known processing site of the *P. denitrificans* subunit II (*22*, *24*). On SDS−PAGE gels (Figure 4), htICcO-16 possesses only one subunit II polypeptide at about the same size as the smaller of the two peptides observed in the wildtype CcO (*1*, *13*). This demonstrates that the incomplete natural processing of subunit II in wildtype *R. sphaeroides* is C-terminal processing, as for the *P. denitrificans* CcO, and does not involve incomplete N-terminal processing (as speculated in ref *1*). Thus htICcO-16 provides a form of *R. sphaeroides* CcO that is easily purified to near-homogeneity (by using the pH 8.0 method as described earlier for htIICcO; data not shown) and therefore potentially suitable for use in crystallization studies.

Effects of Subunit II Modification on Binding to an FPLC DEAE Column. The "artificially processed" htICcO-16 was expected to behave like the natively processed form of the wildtype htICcO (*13*) during FPLC purification, yet it eluted much earlier in the gradient than the processed form of htICcO (Figure 5), indicating less tight binding. Since the DEAE column binds CcO on the basis of the negative charge, and this is concentrated on subunit II (the extra-membrane region of the oxidase), the behavior of htICcO-16 suggests strongly it has less charge in this region. Indeed, in the unpublished crystal structure of the wildtype *R. sphaeroides* oxidase (Iwata, personal communication), subunit II possesses at least two amino acids more than htIICcO-16. Our MALDI-TOF MS data indicate that the natively processed C-terminus of subunit II possesses three additional residues, ending at serine 290. A different location of the C-terminal charge and one more negatively charged amino acid (E288) are apparently responsible for the later elution of the wildtype htICcO in the gradient. Interestingly, htIICcO (22 amino acids removed from the C-terminus plus his-tag added) possesses one less positively charged residue than htICcO-16 or htICcO, yet it binds even less tightly to the FPLC column. This result can be explained by the partially positive his-tag shielding the negatively charged residues necessary for column binding.

There is strong evidence from ion-exchange chromatography studies of the behavior of cytochromes *c* with single charge changes (*32*) that the location of the charge on the protein surface, not the overall charge, determines chromatographic behavior. Thus, it is not unexpected that the natively processed form of the htICcO elutes later in the FPLC gradient than the unprocessed form even though, on the basis of overall charge, the natively processed form should have eluted earlier in the gradient.

Further support for the importance of the position of charges, as opposed to overall charge, in ion-exchange chromatography comes from FPLC purification of three different mutations of carboxyl residues in subunit II (*7*) (Hiser, Zhen, and Ferguson-Miller, unpublished). A D214N mutation, located at the center of the cytochrome *c* binding face of subunit II but hydrogen bonded so it is not exposed (*7*), had little effect on the FPLC elution profile of the CcO, although it removed one negative charge. A E157Q mutation, located 10 Å higher up in the cytochrome *c* binding face (*7*), which also lacks one negative charge, eluted about 2 mL ahead of the wildtype htICcO. A double mutant D151N/E152Q, located 10 Å above E157 and just outside the cytochrome *c* binding face (*7*), lacks two negative charges but actually elutes similarly to the D157N CcO. All of these mutant oxidases elute from the ion-exchange column significantly behind (bind tighter than) htICcO-16, which also lacks one negative charge as compared to the wildtype CcO. It can therefore be concluded that charge location is crucial to the ion-exchange behavior of CcO. A concentration of negative charge toward the top of subunit II may be important, and thus removal of one negative charge in that area (glutamate 288 in htICcO-16) or addition of an obstructing his-tag (htIICcO) has more effect on FPLC purification than charge changes made elsewhere on subunit II.

Effect of C-Terminal Modifications in Subunit II on the Kinetics of Reaction with Cytochrome c. Previous studies have shown that charge changes that most affect ion-exchange chromatographic behavior of modified versions of cytochrome *c* also had the greatest effect on the kinetics of its reaction with CcO (*33*, *34*). The effects of subunit II modification on FPLC purification led us to suspect that similar results might be found for the kinetics of reaction of CcO with cytochrome *c* in this case.

Both the htICcO-16 and the htIICcO appeared to have wildtype activity when assayed polarographically with high concentrations of cytochrome *c* (30 μM) but showed altered kinetics when assayed with subsaturating amounts of substrate (Figure 6, Table 1). The C-terminal modifications in htICcO-16 and htIICcO appear to affect binding to cyto-

chrome *c* in a manner that is qualitatively similar to binding to anion-exchange resin. This is explained by a missing negatively charged glutamate (E288) at the C-terminus of htICcO-16, a change in the exact position of the C-terminal carboxyl group, as well as an interaction of the his-tag itself in htIICcO with negatively charged residues (labeled and shown in green in Figure 3) on the face of subunit II that have been implicated in the binding of cytochrome *c* (*7*, *35*, *36*). Such an interaction of the his-tag is consistent with the need for higher salt in the metal affinity column purification to free the his-tag for interaction with the Ni^{2+}-NTA resin.

The correlation between ion-exchange behavior and altered kinetic parameters also holds true for some, but not all, of the subunit II mutants described by Zhen et al. (*7*). The mutant CcO E157Q (in the center of the cytochrome *c* binding region) and D151N/E152Q (just above the cytochrome *c* binding domain) eluted similarly ahead of the wildtype htICcO in the FPLC gradient (Hiser, Zhen, and Ferguson-Miller, unpublished), but only the E157Q CcO showed altered kinetic parameters (*7*). The htICcO-16 eluted much earlier in the FPLC gradient than the E157Q CcO, but possessed a $K\mathrm{m}_1$ and $V\mathrm{max}_1$ (ref *7* and Table 1) similar to the mutant. Consequently, it can be concluded that slightly different but overlapping sets of negatively charged amino acids are responsible for binding to a DEAE column and for binding to cytochrome *c*. The htICcO-16 data provide an interesting clue that the C-terminal carboxyl of subunit II is involved in both sets; it had not been previously implicated in cytochrome *c* binding. The seeming reduction or elimination of a second kinetic phase in these C-terminally modified CcOs (Figure 6) also supports the idea that the region of the C-terminus carboxyl may be important for a second binding site for cytochrome *c*.

Identification of the Native Processed C-Terminus of Subunit II. The results of chromatography and kinetic analysis clearly identified that the natively processed form of subunit II was not identical to the artificially processed version, in which the processing was the same as for the oxidase from *P. denitrificans*. Mass spectrometry analysis of the two forms definitively showed that there are in fact three more amino acids at the C-terminus of the natively processed *R. sphaeroides* oxidase. The more rapid elution from an anion exchange column and the lower affinity for cytochrome *c* is a larger change than might be expected for removal of a single charge (Glu288), especially one that is expected to be outside the high affinity binding domain for cytochrome *c* (*7*, *37*, *38*). However, the position of the C-terminal carboxyl will also be different and could be an even more important factor. If so, it is noteworthy that the mass spectrometry analysis also identifies in purified wildtype oxidase the form in which the C-terminus is not processed. In all preparations of wildtype *R. sphaeroides* this unprocessed form is seen, and this likely creates inhomogeneity with respect to the cytochrome *c* interaction.

Purification of COVs for Proton Pumping Analysis. The accurate measurement of the proton pumping activity of CcO is difficult and impedes our understanding of its mechanism of energy conservation (*5*). Apart from the problems of reconstituting a purified membrane protein into a lipid bilayer, it is problematic to measure protons in the presence of buffering and light-scattering lipid vesicles. Placing a six-histidine tag on the C-terminus of subunit II of cytochrome *c* oxidase provides a means of purification of COVs by Ni-affinity chromatography, leading to a more concentrated sample of vesicles with correctly oriented CcO and the removal of vesicles devoid of enzyme. Because of the increased protein-to-lipid ratio (we calculate by about 10-fold) in these purified COVs, increased concentrations of oxidase can be used in the spectrophotometric measurements of proton pumping with less buffering and scattering problems. Increasing the concentration of the oxidase permits the observation of proton pumping with fewer turnovers, which normally is found to give better proton-to-electron ratios.

Because of the significantly reduced lipid concentrations, it was expected that there would be increased signal-to-noise in phenol red absorbance measurements for proton uptake and release. Instead, the purification procedure resulted in COVs with similar signal-to-noise but much better correlations between proton and electron transfer rates, something that had previously been variable.

Additionally, in the stopped-flow measurements, purified htII COVs gave rates of cytochrome *c* oxidation and corresponding proton-transfer higher than observed for nonpurified htI COVs, at equivalent concentrations of oxidase and cytochrome *c*. These higher apparent molecular activities (as much as 3-fold) may reflect in part the decreased concentration of charged phospholipid headgroups that can bind the added cytochrome c^{2+} (not at saturating concentrations in the pumping assays) and decrease its availability to react with the cytochrome *c* oxidase as well as decreased kinetic effectiveness of valinomycin and CCCP in complete and rapid release of the membrane potential. The high rates obtained with the purified htII COVs have not been observed in other COV preparations and are closer to the activities obtained with free enzyme. Therefore, this method should considerably enhance our ability to measure proton pumping in a time-resolved fashion with even extremely low activity cytochrome *c* oxidase mutants. Use of a strategically placed his-tag as a method of purifying enzyme-containing vesicles may be useful for the reconstitution of other membrane proteins where protein orientation is otherwise difficult to achieve.

ACKNOWLEDGMENT

We thank Jeff Leipprandt for assistance in FPLC purification of and initial observation of the altered behavior of the htICcO-16 oxidase; Dr. Yuejun Zhen for providing *R. sphaeroides* cytochrome c_2 and protein from the D214N, E157Q, and D151N/E157Q mutants; Dr. Laurence Florens and Dr. Neil Bowlby for assistance in the preparation of Figures 3 and 4, respectively; and Dr. Douglas Gage for helpful discussions.

REFERENCES

1. Hosler, J. P., Espe, M. P., Zhen, Y., Babcock, G. T., and Ferguson-Miller, S. (1995) *Biochemistry 34*, 7586−7592.
2. Fetter, J. R., Qian, J., Shapleigh, J., Thomas, J. W., García-Horsman, J. A., Schmidt, E., Hosler, J., Babcock, G. T., Gennis, R. B., and Ferguson-Miller, S. (1995) *Proc. Natl. Acad. Sci. U.S.A. 92*, 1604−1608.
3. Fetter, J. R., Sharpe, M., Qian, J., Mills, D., Ferguson-Miller, S., and Nicholls, P. (1996) *FEBS Lett 393*, 155−160.

4. Qian, J., Shi, W., Pressler, M., Hoganson, C., Mills, D., Babcock, G. T., and Ferguson-Miller, S. (1997) *Biochemistry 36*, 2539−2543.
5. Mills, D. A., and Ferguson-Miller, S. (1998) *Biochim. Biophys. Acta 1365*, 46−52.
6. Mills, D., Florens, L., Hiser, C., and Ferguson-Miller, S. (2000) *Biochim. Biophys. Acta 1458*, 180−187.
7. Zhen, Y., Hoganson, C. W., Babcock, G. T., and Ferguson-Miller, S. (1999) *J. Biol. Chem. 274*, 38032−38041.
8. Casey, R. P., Chappell, J. B., and Azzi, A. (1979) *Biochem. J. 182*, 149−156.
9. Anthony, G., Reimann, A., and Kadenbach, B. (1993) *Proc. Natl. Acad. Sci. U.S.A. 90*, 1652−1656.
10. Pabarue, H., Parilo, M., Wilson, K. S., Estey, L. A., and Prochaska, L. J. (1997) *Biophys. J. 72*, A318.
11. Madden, T., and Cullis, P. R. (1985) *Biochim. Biophys. Acta 808*, 219−224.
12. Mitchell, D. M., and Gennis, R. B. (1995) *FEBS Lett. 368*, 148−150.
13. Zhen, Y., Qian, J., Follmann, K., Hosler, J., Hayward, T., Nilsson, T., and Ferguson-Miller, S. (1998) *Protein Expr. Purf. 13*, 326−336.
14. Horton, R. M., Hunt, H. D., Ho, S. N., Pullen, J. K., and Pease, L. R. (1989) *Gene 77*, 61−68.
15. Keen, N. T., Tamaki, S., Kobayashi, D., and Trollinger, D. (1988) *Gene 70*, 191−197.
16. Shapleigh, J., Hosler, J., Tecklenburg, M., Kim, Y., Babcock, G., Gennis, R., and Ferguson-Miller, S. (1992) *Proc. Nat. Acad. Sci. U.S.A. 89*, 4786−4790.
17. Cao, J., Hosler, J., Shapleigh, J., Gennis, R., Revzin, A., and Ferguson-Miller, S. (1992) *J. Biol. Chem. 267*, 24273−24278.
18. Sistrom, W. R. (1962) *J. Gen. Microbiol. 28*, 607−616.
19. Hosler, J. P., Fetter, J., Tecklenburg, M. M. J., Espe, M., Lerma, C., and Ferguson-Miller, S. (1992) *J. Biol. Chem. 267*, 24264−24272.
20. Peiffer, W. E., Ingle, R. T., and Ferguson-Miller, S. (1990) *Biochem. 29*, 8698−9701.
21. Vanneste, W. H. (1966) *Biochemistry 5*, 838−848.
22. Steinrucke, P., Steffens, G. C. M., Panskus, G., Buse, G., and Ludwig, B. (1987) *Eur. J. Biochem. 167*, 431−439.
23. Tsukihara, T., Aoyama, H., Yamashita, E., Tomizaki, T., Yamaguchi, H., Shinzawa-Itoh, K., Nakashima, R., Yaono, R., and Yoshikawa, S. (1996) *Science 272*, 1136−1144.
24. Iwata, S., Ostermeier, C., Ludwig, B., and Michel, H. (1995) *Nature 376*, 660−669.
25. Ferguson-Miller, S., Brautigan, D., and Margoliash, E. (1976) *J. Biol. Chem 251*, 1104−1115.
26. Rigaud, J., Pitard, B., and Levy, D. (1995) *Biochem. Biophys. Acta 1231*, 223−246.
27. Tihova, M., Tattrie, B., and Nicholls, P. (1993) *Biochem. J. 292*, 933−946.
28. Casey, R. P., O'Shea, P. S., Chappell, J. B., and Azzi, A. (1984) *Biochim. Biophys. Acta 765*, 30−37.
29. Gregory, L., and Ferguson-Miller, S. (1989) *Biochemistry 28*, 2655−2662.
30. Nicholls, P., Hildebrandt, V., and Wrigglesworth, J. (1980) *Arch. Biochem. Biophys. 204*, 533−543.
31. Mitchell, D. M., Fetter, J. R., Mills, D. A., Adelroth, P., Pressler, M. A., Kim, Y., Aasa, R., Brzezinski, P., Malmstrom, B. G., Alben, J. O., Babcock, G. T., Ferguson-Miller, S., and Gennis, R. B. (1996) *Biochemistry 35*, 13089−93.
32. Brautigan, D. L., Ferguson-Miller, S., and Margoliash, E. (1978) *J. Biol. Chem. 253*, 130−9.
33. Brautigan, D. L., Ferguson-Miller, S., Tarr, G. E., and Margoliash, E. (1978) *J. Biol. Chem. 253*, 140−8.
34. Ferguson-Miller, S., Brautigan, D. L., and Margoliash, E. (1978) *J. Biol. Chem. 253*, 149−159.
35. Lappalainen, P., Watmough, N. J., Greenwood, C., and Saraste, M. (1995) *Biochemistry 34*, 5824−5830.
36. Witt, H., Malatesta, F., Nicoletti, F., Brunori, M., and Ludwig, B. (1998) *Eur. J. Biochem. 251*, 367−73.
37. Wang, K., Zhen, Y., Sadoski, R., Grinnell, S., Geren, L., Ferguson-Miller, S., Durham, B., and Millett, F. (1999) *J. Biol. Chem. 274*, 38042−38050.
38. Roberts, V. A., and Pique, M. E. (1999) *J. Biol. Chem. 274*, 38501−38509.

BI0018988